RADAR/INS TIGHTLY-COUPLED INTEGRATION FOR LAND VEHICLE NAVIGATION

M. Elkholy[1,2*], M. Elsheikh[1,3], N. El-Sheimy[1]

[1] Department of Geomatics Engineering, University of Calgary, Calgary, Alberta, Canada – (mohamed.elkholy, mohamed.elsheikh, elsheimy)@ucalgary.ca
[2] Department of Transportation Engineering, Faculty of Engineering, Alexandria University, Alexandria, Egypt.
[3] Department of Electronics and Communication Engineering, Tanta University, Egypt.

KEY WORDS: FMCW Radar –Inertial Navigation System - GNSS Outage - Radar/INS Integration – Tightly Coupled Integration.

ABSTRACT:

Multisensor systems are essential for autonomous navigation applications to achieve reliable accuracy. Integrating the Global Navigation Satellite System (GNSS) and the Inertial Navigation System (INS) is the most common integration scheme. However, this integration is unreliable in different scenarios since the GNSS signal may deteriorate in downtown areas or suffer from a blockage in underground and indoor areas. Therefore, other sensors are integrated with INS to compensate for GNSS outages. This paper proposes a novel algorithm for radar/INS tightly-coupled integration for autonomous navigation applications. This algorithm is applied in multiple steps. Radar data analysis is the first and most crucial step to remove the noisy data and the outliers and keep the useful objects. Then, data association is done to match the detected objects between radar frames. The tightly-coupled integration is performed at the measurement level through an Extended Kalman Filter (EKF), where the distance between the INS and the detected objects can be predicted from the INS and measured from the radar. Real data was collected from four Frequency Modulated Continuous Wave (FMCW) radar units in Calgary's suburban areas and Toronto's downtown area. The proposed algorithm was tested and assessed by introducing simulated GNSS single outages with different durations. The results show an enhancement in the vehicle's position by about 94% to 96%.

1. INTRODUCTION

GNSS is an all-weather navigation system that can estimate the vehicle's position with centimeter-level accuracy(Suzuki, 2020). However, GNSS is not reliable in some scenarios or applications, e.g., indoor and underground parking lots, driving through canyons, or in downtown areas where the GNSS signal is blocked or deteriorates due to multipath effects (P. Xie & Petovello, 2015). On the other hand, INS is a dead reckoning system that can estimate the vehicle's relative position, velocity, and attitude with high accuracy but for a short period since the INS solution drifts with time. Therefore, GNSS and INS are integrated to compensate for GNSS outages and overcome INS errors (Chen et al., 2021). Loosely-Coupled and Tightly-Coupled are the most known integration techniques in autonomous navigation (Dong et al., 2020; R. Xu et al., 2018). However, in the case of a long GNSS signal outage, the dependency on INS as a standalone sensor to estimate the vehicle's navigation state is not sufficient. Thus, INS is integrated with other sensors to overcome INS errors and drift. For example, the magnetometer can be an update source to the vehicle's heading angle. However, it is affected by the surrounding magnetic field (Cui et al., 2021; Wu & Wang, 2019). The onboard sensors, e.g., the odometer, measure the vehicle's forward speed and can aid the inertial measurement unit (IMU) (Kim & Bae, 2019). Odometer is affected by slippery roads and unequal tire pressure.

Light detection and ranging (lidar) is used to detect the surrounding environments. Now, lidar is integrated with INS for autonomous vehicle applications and simultaneous localization and mapping (SLAM) (Chang et al., 2019; Zou et al., 2022). Nevertheless, lidar is affected by different weather conditions, such as fog and rainy weather. Moreover, it requires high computational power due to its dense point clouds. Furthermore, lidar is a high-cost sensor.

Vision sensors or cameras use visible light to detect and track objects. Moreover, vision sensors can detect road lanes and traffic signs (Jia et al., 2006; Xing et al., 2018). However, vision sensors are affected by varying light and weather conditions because they cannot work in dark or foggy weather.

On the other hand, radio detection and ranging (radar) is known as an all-weather sensor, and it is the only sensor, in addition to INS, that can work in different weather and light conditions. Therefore, this paper studies the integration between radar and INS to estimate the vehicle's navigation state.

This paper is organized as follows: Section 2 contains the related work, whereas the methodology is described in Section 3. Section 4 discusses the experimental work and results, and finally, the conclusion is shown in Section 5.

2. RELATED WORK

There are two main types of radar: 360º radar and static radar. The 360º radar, known as the imaging radar, rotates 360 degrees to scan the surrounding environment. The 360º radar measures only the point location of detected objects represented by its range and azimuth angle and provides the intensity value for each point. Due to the continuous movement of the vehicle and the rotation of the radar unit, the point clouds are distorted, and they need to be corrected.

In contrast, the static radar has a specific field of view and higher frequency than the 360º radar unit. Moreover, it provides information about the location of the detected points (range and bearing angle) and the Doppler frequency information between the radar unit and the point clouds. The static radar is also known

* Corresponding author

as the Frequency Modulated Continuous Wave (FMCW) radar. The Doppler frequency information can be used to estimate the relative velocity between the radar unit and each point, which can help differentiate between static and moving objects.

There are different studies about using radar to estimate the vehicle's pose. These studies can be divided into two categories: radar scan matching and feature detection and matching. The Iterative Closest Point (ICP) is the most common technique in radar scan matching. It depends on minimizing the distance between point clouds to estimate the transition and rotation between successive radar frames (Censi, 2008; X. Xu et al., 2018). Normal Distribution Transform (NDT) builds a normal distribution model for one point cloud in each frame. These models are matched together to estimate the vehicle's pose (Biber & Strasser, n.d.). Fourier Mellin Transform (FMT) is another scan-matching technique (Checchin et al., 2010).

For feature detection and matching, Scale-Invariant Feature Transform (SIFT), Speeded-Up Robust Features (SURF), and Oriented fast and Rotated Brief (ORB) are common methods in image processing to detect and extract the features, build the descriptor for each feature, and match these features together (Rublee et al., 2011; S. Xie et al., 2013). Thus, the transition and rotation between successive radar frames can be estimated. Constant False Alarm Rate (CFAR) is another technique to detect and keep the actual features by applying a moving filter to remove the noise and the outliers (Rohling, 2011).

In (Cen & Newman, 2018), a 360º radar unit was employed, and a median filter, binominal filter, and threshold were adopted to remove the outliers and ghost points and keep the real features. The unary descriptor and Euclidean distance between the features were applied for data association.

The radar solution can be integrated with IMU to improve navigation solution accuracy and robustness and limit IMU drift. (Elkholy et al., 2022) applied the ORB algorithm on 360º radar data to detect and match the features to estimate the vehicle's relative position. The radar solution was integrated with IMU through a closed-loop EKF to correct the navigation states.

In (Elkholy et al., 2022), four static radar units were used for land vehicle navigation applications. The four radar units were mounted on the vehicle's roof to act as one 360º radar unit. With the knowledge of the vehicle's average speed and radar rate, the data association between radar frames can be applied, and the vehicle's ego motion can be estimated. The radar solution was integrated with INS through an EKF to estimate the vehicle's position in the GNSS-denied environments.

Radar can be used to estimate the vehicle's forward speed. Therefore, radar can also be integrated with the Reduced Inertial Sensor System (RISS). RISS uses two accelerometer sensors and one gyroscope. In (Abosekeen et al., 2018), the FMCW radar unit was mounted on the vehicle's front bumper and facing the ground. The estimated relative speed between the radar unit and the ground represents the vehicle's forward speed. The estimated vehicle's forward speed was integrated with RISS through an EKF. (Dawson et al., 2022) exploited two radar units mounted on the vehicle's top roof to detect static objects and estimate the vehicle's forward velocity. The radar solution was integrated with RISS to compensate for GNSS outages.

In (Mohamed Elkholy et al., 2023), four radar units were mounted on the vehicle's roof. The two radar units at the front were used to estimate the vehicle's forward velocity, while all four units were used to estimate the vehicle's ego-motion. Then, two EKFs were applied. One was to integrate the radar solution with an IMU, and the second was to correct the integrated position by applying map matching. In (Almalioglu et al., 2021), the Millimeter-wave (MMwave) Radar was integrated with the IMU sensor through Unscented Kalman Filter (UKF) for indoor applications. To remove radar noise and IMU biases, the NDT with angular velocity from the IMU sensor was adopted. (Kwon et al., 2021) utilized FMCW radar to estimate the velocity for unmanned aerial vehicle applications. Radar velocity was integrated with IMU through an Adaptive EKF.

All the previous research provided examples of loosely coupled integration between radar and INS. However, there is no previous research that focuses on the tightly coupled integration between radar and INS.

This paper proposes a novel radar/INS tightly-coupled integration algorithm to compensate for GNSS outages and overcome INS errors and drift. Closed-loop EKF was exploited to implement the radar/INS integration.

3. METHODOLOGY

The methodology of this research is applied in multiple steps. The first and most crucial step is data analysis and preprocessing since radar data is noisy and contains outliers and ghost points, which could affect the proposed algorithm. Therefore, the preprocessing technique is adopted to remove all the outliers and moving objects and detect and keep only the static objects. After that, the data association technique is applied to match the detected static objects between radar frames. The detected objects are matched by applying motion and distance constraints to find the corresponding points between radar frames. Finally, the Radar measurements are integrated in a tightly-coupled mode with predicted IMU measurements to provide a continuous, robust Radar/INS solution.

3.1. Data Analysis and Preprocessing

Radar data analysis is a crucial step in the proposed algorithm since data analysis and preprocessing aim to remove all the outliers, ghost points, and moving objects that will affect the following steps.

The radar data analysis is performed in multiple steps. The first step is to differentiate between static and moving objects. FMCW radar provides Doppler frequency information, which can be used to estimate the relative velocity between the vehicle and the surrounding objects. For example, if the vehicle is static, the relative velocity between the vehicle and the surrounding static objects should be zero, and if the vehicle is moving, the relative velocity between the vehicle and the static objects equals the vehicle speed. Moreover, in this research, four FMCW radar units were used and mounted on the vehicle's roof to work as a 360º radar. If the vehicle is moving forward, static objects detected by the two front radar units will appear coming toward the vehicle, and the relative velocity sign is negative, whereas the static objects detected by the two rear radar units will appear to move away from the vehicle and the relative velocity sign between the vehicle and the detected objects is positive.

The previous technique is valid when the vehicle is moving forward. However, if the vehicle moves backward, the relative velocity sign between the vehicle and the detected objects from the four radar units will be reversed. The heading angle difference can be utilized to check if the vehicle changed its moving direction. If there is a large drop (about 180º) in the vehicle's heading angle and the vehicle was statice before that drop, that means that the vehicle was moving in a specific direction and now the vehicle is moving in the opposite direction.

To improve the previous technique in detecting the static objects and removing the moving objects, a median filter was applied to check if there are moving objects were detected and remove them.

The detected static objects are filtered by removing the close and far points as they are considered outliers. Moreover, an intensity threshold is applied to remove the outliers.

3.2. Data Association

After detecting and filtering the static objects and removing the outliers and the moving objects, the next step is to find the corresponding objects in the following Radar frame. The proposed method for data association is based on point-to-point matching. The change in azimuth, range, and elevation angle between the corresponding objects can be considered with the knowledge of radar data rate and the average vehicle speed. Therefore, the range, bearing angle, and elevation angle difference between any two corresponding objects should be less than a threshold. Moreover, the rotation angles of all the matched points should be similar to a certain threshold. Then, the corresponding points can be related.

3.3. Radar/INS Tightly Coupled Integration

Figure 1 shows the block diagram of the proposed tightly-coupled Radar/INS integration. The detected objects' coordinates are measured in the radar frame. Since the lever arm and boresight angle between the radar frame and IMU frame are measured, the detected objects' coordinates can be transformed into the IMU/body frame or the vehicle frame because the IMU frame is aligned with the vehicle frame.

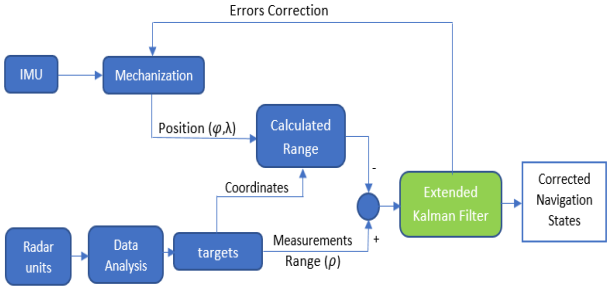

Figure 1. Radar/INS tightly coupled integration technique.

Assume that the vehicle's position (INS position) is represented by the latitude (φ_{INS}^{t}) and longitude (λ_{INS}^{t}) at a time (t). Then, with the knowledge of the coordinates of the target points, the target points' latitude (φ_{PC}^{t}) and longitude (λ_{PC}^{t}) at a time (t) can be calculated.

$$\varphi_{PC}^{t} = \varphi_{INS}^{t} + \frac{y}{Rm + h_{INS}^{t}} \quad (1)$$

$$\lambda_{PC}^{t} = \lambda_{INS}^{t} + \frac{x}{(Rm + h_{INS}^{t})\cos\varphi_{INS}^{t}} \quad (2)$$

where: (x, y) are the target point coordinates to the INS in the INS body frame, h_{INS}^{t} is the height at time (t), and Rm is the meridian radius of the earth.

At the time $(t + \Delta t)$, the corresponding target points have the same latitude (φ_{PC}^{t}) and longitude (λ_{PC}^{t}). To correct the navigation state at the time $(t + \Delta t)$, the range between point clouds and the vehicle's position (ρ_{INS-PC}) can be calculated. The calculated range should be equal to the range given by Radar data.

$$\rho_{INS-PC} = \sqrt{(\varphi_{INS}^{t+\Delta t} - \varphi_{PC}^{t})^2 + (\lambda_{INS}^{t+\Delta t} - \lambda_{PC}^{t})^2} \quad (3)$$

The tightly coupled integration is implemented through a closed-loop EKF. The EKF consists of two models (the motion model and the measurement mode).

The system model in the continuous case is described as follows:

$$\dot{x} = Fx + Gw \quad (4)$$

where: $\dot{x}$ = the time rate of change of the state vector.
F = dynamic matrix.
x = state vector.
G = noise coefficient matrix.
w = system noise.

The measurement model is described by:

$$z = \rho_{INS-PC} - \rho_{Radar} = Hx + \eta \quad (5)$$

where: z = the measurements.
H = the design matrix.
η = the measurement noise.

If there are multiple detected objects (n), the measurements will be as follows:

$$z = \begin{bmatrix} (\rho_{INS-PC})_1 - (\rho_{Radar})_1 \\ \vdots \\ (\rho_{INS-PC})_n - (\rho_{Radar})_n \end{bmatrix} \quad (6)$$

The design matrix (H) in this case will be as follows:

$$H = \begin{bmatrix} \frac{\varphi_{INS}^{t+\Delta t} - (\varphi_{PC}^{t})_1}{(\rho_{INS-PC})_1} & \frac{\lambda_{INS}^{t+\Delta t} - (\lambda_{PC}^{t})_1}{(\rho_{INS-PC})_1} & 0_{1x13} \\ \vdots & \vdots & \vdots \\ \frac{\varphi_{INS}^{t+\Delta t} - (\varphi_{PC}^{t})_n}{(\rho_{INS-PC})_n} & \frac{\lambda_{INS}^{t+\Delta t} - (\lambda_{PC}^{t})_n}{(\rho_{INS-PC})_n} & 0_{1x13} \end{bmatrix} \quad (7)$$

EKF is implemented in two stages. The first stage is to predict the state vector at time t+Δt.

$$x'_{t+\Delta t} = \emptyset x_t + w_t \quad (8)$$

$$p'_{t+\Delta t} = \emptyset p_t \emptyset^T + Q_t \quad (9)$$

where: $x'_{t+\Delta t}$ = the predicted state vector at the time (t+Δt).
$\emptyset$ = the transition matrix.
x_t = the state vector at the time (t).
$p'_{t+\Delta t}$ = the predicted covariance matrix at the time (t+Δt).
p_t = the covariance matrix at the time (t).
w_t = the system noise at the time (t).
Q_t = the process noise matrix.

The second stage is to update the state based on the measurements.

$$K_{t+\Delta t} = p'_{t+\Delta t} H_{t+\Delta t}^{T} (H_{t+\Delta t} p'_{t+\Delta t} H_{t+\Delta t}^{T} + R_{t+\Delta t})^{-1} \quad (10)$$

$$\hat{x}_{t+\Delta t} = x'_{t+\Delta t} + K_{t+\Delta t}(Z_{t+\Delta t} - H_{t+\Delta t} x'_{t+\Delta t}) \quad (11)$$

$$\hat{p}_{t+\Delta t} = [\mathrm{I} - K_{t+\Delta t} H_{t+\Delta t}]\, p'_{t+\Delta t} \quad (12)$$

where: $K_{t+\Delta t}$ = the gain matrix.
$R_{t+\Delta t}$ = the covariance matrix of the measurement noise.
$\hat{x}_{t+\Delta t}$ = the updated state vector.
$\hat{p}_{t+\Delta t}$ = the updated covariance matrix of the state vector.

So, the system model is the core of the prediction stage where the state vector and the covariance matrix can be predicted. The updated stage is based on calculating the gain matrix which depends on the predicted covariance matrix of the state vector, the design matrix, and the covariance matrix of the measurements. Finally, the updated state vector and the updated covariance matrix are calculated from the predicted ones and the updated measurements.

The novel algorithm has the advantage that it can work with only one target point and its corresponding point in the second Radar frame to be implemented.

4. EXPERIMENTAL WORK AND RESULTS

Two real driving datasets were collected to test the proposed algorithm. The first dataset was collected in a suburban area in Calgary. Four FMCW UMRR-11 Type 132 were mounted on the vehicle's roof. Xsens MTI-G-710 module was used to collect IMU and GNSS data. For reference data, a Novatel SPAN-SE system with an IMU-FSAS was used (**Figure *2***). Another data was collected in downtown Toronto. Four FMCW UMRR-96 Type 153 radar units were used. In addition, the u-blox ZED-F9R module was used to collect the IMU and GNSS measurements. Finally, the reference data were collected by a Novatel PwrPak7 system with an IMU-KVH1750.

Figure 2. The setup of radar units and Xsens MTI-G-710 during data collection in Calgary.

The data association and matching algorithm was implemented. Figure 3 shows the matching results between two successive radar frames.

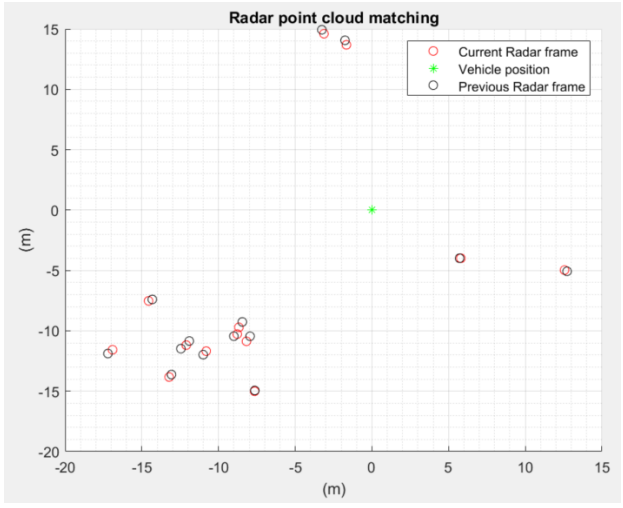

Figure 3. An example of matching points between two successive radar frames.

After applying the data association algorithm, The radar/INS tightly coupled integration was implemented, and a simulated GNSS signal outage was introduced for different outage durations. The GNSS outage durations range from 30 seconds to 120 seconds.

4.1. Calgary Data

The proposed algorithm was applied to Calgary's data to compensate for the GNSS signal outage. Figure 4 shows the proposed integrated solution during a simulated two-minute GNSS signal outage.

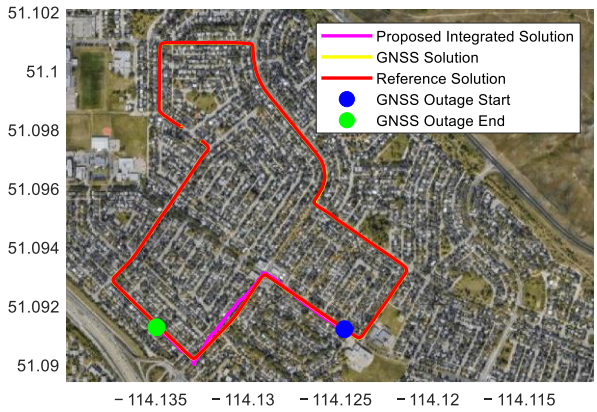

Figure 4. The estimated trajectory from radar/INS tightly coupled integration during a simulated GNSS outage in Calgary data.

Table 1 shows the RMSE from the radar/INS tightly coupled integration algorithm and the INS standalone solution during different GNSS signal outage durations.

Table 1. RMSE from radar/INS tightly coupled integration and INS standalone solution.

Outage Duration	RMSE (m)		Traveled Distance (m)
	INS Standalone	Radar/INS	
30 sec	6.65	4.8	342.5
60 sec	11.62	4.94	415.85
90 sec	122.15	5.8	722.55
120 sec	255.1	9.57	977.49

From Table 1, the proposed integration algorithm enhanced the vehicle's horizontal position by 27.82% and 57.49% for 30-second and 60-second GNSS signal outage durations, respectively. For 90 seconds and two minutes of GNSS signal outages, the horizontal position was improved by 95.25% and 96.25%, respectively. The average percentage error from the proposed algorithm was 1.09%, and the traveled distance was about 1 km.

Another simulated GNSS signal outage was introduced, as shown in Figure 5. Table 2 illustrates the horizontal RMSE from the INS standalone solution and the proposed algorithm where it shows the enhancement in the vehicle's horizontal position after applying the radar/INS tightly coupled integration algorithm. The horizontal position was improved by 95.65% for 30 second GNSS signal outage and by 86.95% for 60 second GNSS signal outage. For 90 seconds and 120 seconds of GNSS signal outages,

the vehicle's horizontal was improved by 92.57% and 94.38%, respectively. The average percentage error was 2.09%, and the traveled distance was 802.33 m.

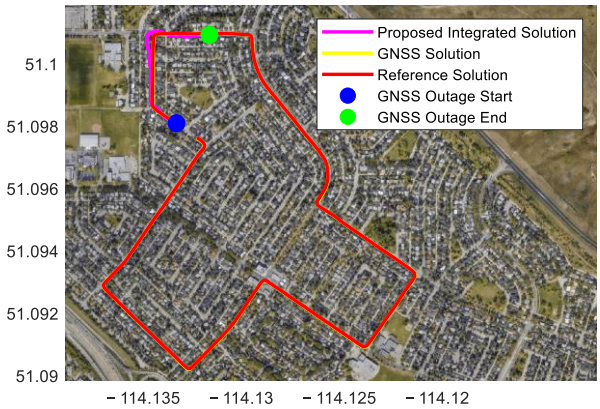

Figure 5. The estimated trajectory from the proposed algorithm during another simulated GNSS outage in Calgary data.

Table 2. RMSE from radar/INS tightly coupled integration and INS standalone solution.

Outage Duration	RMSE (m)		Traveled Distance (m)
	INS Standalone	Radar/INS	
30 sec	67.6	2.94	154.6
60 sec	91.55	11.95	350.14
90 sec	119.78	8.9	575.58
120 sec	219.05	12.3	802.33

4.2. Toronto Data

For the Toronto dataset, the proposed algorithm was tested, and a simulated GNSS signal outage was introduced (Figure 6). Table 3 illustrates the improvements in the vehicle's position after the integration between radar and INS.

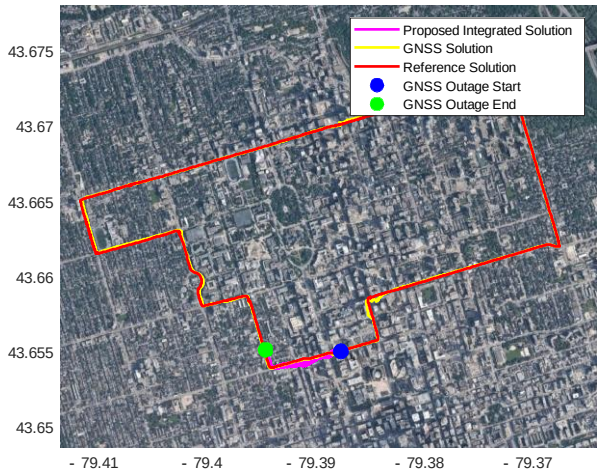

Figure 6. The estimated trajectory from radar/INS tightly coupled integration during a simulated GNSS outage in Toronto data.

Table 3 shows the horizontal position enhancement after applying the tightly coupled integration between radar and INS. For 30-second and 60-second GNSS signal outages, the position improved by about 82% and 92.06%, respectively. Moreover, the vehicle's horizontal position was enhanced by 93.64% for the 90-second GNSS signal outage and 94.12% for the two-minute GNSS signal outage. The average percentage error was about 4%, and the traveled distance was 743 m.

Table 3. RMSE from radar/INS integration solution and INS standalone solution for Toronto data.

Outage Duration	RMSE (m)		Traveled Distance (m)
	INS Standalone	Radar/INS	
30 sec	60.18	10.84	176.26
60 sec	192.14	15.25	456.47
90 sec	304.77	19.38	527.01
120 sec	366.53	21.45	743.16

From the previous results, the proposed algorithm improved the vehicle's navigation solution. However, the accuracy of the vehicle's position depends on radar data uncertainties, the detection of static objects, and the efficiency of the matching technique between radar frames. Therefore, there is a great enhancement in the Calgary dataset during the first GNSS signal outage and a slight improvement during the other GNSS signal outages.

5. CONCLUSION

This paper proposes a novel algorithm for tightly coupled integration between radar and INS for land vehicle navigation applications in GNSS-denied environments. Four FMCW radar units were mounted on the vehicle's roof and utilized to test the proposed algorithm. Data analysis and preprocessing were implemented on radar data to detect the static objects and remove the outliers and moving objects. The detected static objects were matched to find the corresponding points. The range between the detected static objects and INS can be calculated and updated through EKF to achieve tightly coupled integration between radar and INS. The proposed algorithm improved the vehicle's horizontal position during different GNSS signal outages. The horizontal position accuracy was improved by an average of 95%, and the average percentage RMS error was about 2.3%. Moreover, the proposed algorithm has the advantage that one matched static object between two successive radar frames is enough to apply this algorithm and limit the IMU drifts. However, there are some limitations in this research. Since radar data is so noisy, data analysis, preprocessing, and data association are critical and affect the vehicle's position accuracy. Better pre-analysis and matching techniques need to be considered to improve the vehicle's position accuracy, and applying other filtering techniques could help to improve the position's accuracy.

ACKNOWLEDGMENTS

The authors would like to thank the Navigation and Instrumentation Research Lab (NAVINST) at the Royal Military College of Canada for collecting and sharing the Toronto data.
This research has been supported by funding from Prof. Naser El-Sheimy from NSERC CREATE and Canada Research Chairs programs.

REFERENCES

Abosekeen, A., Noureldin, A., Korenberg, M. J. 2018: Utilizing the ACC-FMCW radar for land vehicles navigation. *2018 IEEE/ION Position, Location and Navigation Symposium, PLANS 2018 - Proceedings*, 124–132. https://doi.org/10.1109/PLANS.2018.8373373

Almalioglu, Y., Turan, M., Lu, C. X., Trigoni, N., Markham, A. 2021: Milli-RIO: Ego-Motion Estimation with Low-Cost Millimetre-Wave Radar. *IEEE Sensors Journal*, *21*(3), 3314–3323. https://doi.org/10.1109/JSEN.2020.3023243

Biber, P., Strasser, W. (n.d.). 2003: The normal distributions transform: a new approach to laser scan matching. *Proceedings 2003 IEEE/RSJ International Conference on Intelligent Robots and Systems (IROS 2003) (Cat. No.03CH37453)*, *3*, 2743–2748. https://doi.org/10.1109/IROS.2003.1249285

Cen, S. H., Newman, P. 2018: Precise Ego-Motion Estimation with Millimeter-Wave Radar under Diverse and Challenging Conditions. *Proceedings - IEEE International Conference on Robotics and Automation*, 6045–6052. https://doi.org/10.1109/ICRA.2018.8460687

Censi, A. 2008: An ICP variant using a point-to-line metric. *2008 IEEE International Conference on Robotics and Automation*, 19–25.

Chang, L., Niu, X., Liu, T., Tang, J., Qian, C. 2019: GNSS/INS/LiDAR-SLAM Integrated Navigation System Based on Graph Optimization. In *Remote Sensing*. Vol. 11, Issue 9. https://doi.org/10.3390/rs11091009

Checchin, P., Gérossier, F., Blanc, C., Chapuis, R., Trassoudaine, L. 2010: *Radar Scan Matching SLAM Using the Fourier-Mellin Transform BT - Field and Service Robotics* (A. Howard, K. Iagnemma, & A. Kelly (eds.); pp. 151–161). Springer Berlin Heidelberg.

Chen, Q., Zhang, Q., Niu, X. 2021: Estimate the Pitch and Heading Mounting Angles of the IMU for Land Vehicular GNSS/INS Integrated System. *IEEE Transactions on Intelligent Transportation Systems*, *22*(10), 6503–6515. https://doi.org/10.1109/TITS.2020.2993052

Cui, X., Li, Y., Wang, Q., Karaim, M., Noureldin, A. 2021: Vehicle heading estimation of INS/magnetometer integrated system based on constant hard iron interference calibration. *Measurement and Control (United Kingdom)*, *54*(7–8), 1208–1218. https://doi.org/10.1177/00202940211021876

Dawson, E., Rashed, M. A., Abdelfatah, W., Noureldin, A. 2022: Radar-Based Multisensor Fusion for Uninterrupted Reliable Positioning in GNSS-Denied Environments. *IEEE Transactions on Intelligent Transportation Systems*, *23*(12), 23384–23398. https://doi.org/10.1109/TITS.2022.3202139

Dong, Y., Wang, D., Zhang, L., Li, Q., Wu, J. 2020: Tightly Coupled GNSS/INS Integration with Robust Sequential Kalman Filter for Accurate Vehicular Navigation. In *Sensors*. Vol. 20, Issue 2. https://doi.org/10.3390/s20020561

Elkholy, M., Elsheikh, M., El-Sheimy, N. 2022: Radar/Ins Integration for Pose Estimation in Gnss-Denied Environments. *The International Archives of the Photogrammetry, Remote Sensing and Spatial Information Sciences*, *XLIII-B1-2*(June), 137–142. https://doi.org/10.5194/isprs-archives-xliii-b1-2022-137-2022

Elkholy, M., Elsheikh, M., El-Sheimy, N. 2022: Radar/IMU Integration Using Visual Feature Matching. *Proceedings of the 35th International Technical Meeting of the Satellite Division of The Institute of Navigation (ION GNSS+ 2022)*, 1999–2010. https://doi.org/10.33012/2022.18549

Elkholy, M., Elsheikh, M., El-Sheimy, N. 2023: Radar/INS Integration and Map Matching for Land Vehicle Navigation in Urban Environments. In *Sensors*. Vol. 23, Issue 11. https://doi.org/10.3390/s23115119

Jia, Z., Balasuriya, A., Challa, S. 2006: Recent Developments in Vision Based Target Tracking for Autonomous Vehicles Navigation. *2006 IEEE Intelligent Transportation Systems Conference*, 765–770. https://doi.org/10.1109/ITSC.2006.1706834

Kim, H.-U., Bae, T.-S. 2019: Deep Learning-Based GNSS Network-Based Real-Time Kinematic Improvement for Autonomous Ground Vehicle Navigation. *Journal of Sensors*, *2019*, 3737265. https://doi.org/10.1155/2019/3737265

Kwon, Y. S., Kim, Y. H., Do, H. V, Kang, S. H., Kim, H. J., Song, J. W. 2021: Radar Velocity Measurements Aided Navigation System for UAVs. *2021 21st International Conference on Control, Automation and Systems (ICCAS)*, 472–476. https://doi.org/10.23919/ICCAS52745.2021.9649866

Rohling, H. 2011: Ordered statistic CFAR technique - an overview. *2011 12th International Radar Symposium (IRS)*, 631–638.

Rublee, E., Rabaud, V., Konolige, K., Bradski, G. 2011: ORB: An efficient alternative to SIFT or SURF. *Proceedings of the IEEE International Conference on Computer Vision*, 2564–2571. https://doi.org/10.1109/ICCV.2011.6126544

Suzuki, T. 2020: Time-Relative RTK-GNSS: GNSS Loop Closure in Pose Graph Optimization. *IEEE Robotics and Automation Letters*, *5*(3), 4735–4742. https://doi.org/10.1109/LRA.2020.3003861

Wu, Z., Wang, W. 2019: INS/magnetometer integrated positioning based on neural network for bridging long-time GPS outages. *GPS Solutions*, *23*(3), 88. https://doi.org/10.1007/s10291-019-0877-4

Xie, P., Petovello, M. G. 2015: Measuring GNSS Multipath Distributions in Urban Canyon Environments. *IEEE Transactions on Instrumentation and Measurement*, *64*(2), 366–377. https://doi.org/10.1109/TIM.2014.2342452

Xie, S., Zhang, W., Ying, W., Zakim, K. 2013: Fast detecting moving objects in moving background using ORB feature matching. *Proceedings of the 2013 International Conference on Intelligent Control and Information Processing, ICICIP 2013*, 304–309. https://doi.org/10.1109/ICICIP.2013.6568087

Xing, Y., Lv, C., Chen, L., Wang, H., Wang, H., Cao, D., Velenis, E., Wang, F.-Y. 2018: Advances in Vision-Based Lane Detection: Algorithms, Integration, Assessment, and Perspectives on ACP-Based Parallel Vision. *IEEE/CAA Journal of Automatica Sinica*, *5*(3), 645–661. https://doi.org/10.1109/JAS.2018.7511063

Xu, R., Ding, M., Qi, Y., Yue, S., Liu, J. 2018: Performance Analysis of GNSS/INS Loosely Coupled Integration Systems under Spoofing Attacks. In *Sensors*. Vol. 18, Issue 12. https://doi.org/10.3390/s18124108

Xu, X., Luo, M., Tan, Z., Zhang, M. 2018: Improved ICP Matching Algorithm Based on Laser Radar and IMU. *2018 5th IEEE International Conference on Cloud Computing and Intelligence Systems (CCIS)*, 517–520.

Yanase, R., Hirano, D., Aldibaja, M., Yoneda, K., Suganuma, N. 2022: LiDAR- and Radar-Based Robust Vehicle Localization with Confidence Estimation of Matching Results. In *Sensors*. Vol. 22, Issue 9. https://doi.org/10.3390/s22093545

Zou, Q., Sun, Q., Chen, L., Nie, B., Li, Q. 2022: A Comparative Analysis of LiDAR SLAM-Based Indoor Navigation for Autonomous Vehicles. *IEEE Transactions on Intelligent Transportation Systems*, *23*(7), 6907–6921. https://doi.org/10.1109/TITS.2021.3063477